ARMY RESEARCH LABORATORY

Modeling, Fabrication, and Testing of a Piezoelectric MEMS Vibrational Energy Reclamation Device

by Jeffrey S. Pulskamp

ARL-TR-3442 February 2005

NOTICES

Disclaimers

The findings in this report are not to be construed as an official Department of the Army position unless so designated by other authorized documents.

Citation of manufacturer's or trade names does not constitute an official endorsement or approval of the use thereof.

Destroy this report when it is no longer needed. Do not return it to the originator.

Army Research Laboratory
Adelphi, MD 20783-1197

ARL-TR-3442 **February 2005**

Modeling, Fabrication, and Testing of a Piezoelectric MEMS Vibrational Energy Reclamation Device

Jeffrey S. Pulskamp
Sensors and Electron Devices Directorate, ARL

REPORT DOCUMENTATION PAGE

Form Approved
OMB No. 0704-0188

1. REPORT DATE *(DD-MM-YYYY)*	**2. REPORT TYPE**	**3. DATES COVERED (From - To)**
February 2005	Summary	Annual

4. TITLE AND SUBTITLE	
Modeling, Fabrication, and Testing of a Piezoelectric MEMS Vibrational Energy Reclamation Device	**5a. CONTRACT NUMBER**
	5b. GRANT NUMBER
	5c. PROGRAM ELEMENT NUMBER
6. AUTHOR(S)	**5d. PROJECT NUMBER**
Jeffrey S. Pulskamp	**5e. TASK NUMBER**
	5f. WORK UNIT NUMBER
7. PERFORMING ORGANIZATION NAME(S) AND ADDRESS(ES)	**8. PERFORMING ORGANIZATION REPORT NUMBER**
U.S. Army Research Laboratory ATTN: AMSRD-ARL-SE-RL 2800 Powder Mill Road Adelphi, MD 20783-1197	ARL-TR-3442
9. SPONSORING/MONITORING AGENCY NAME(S) AND ADDRESS(ES)	**10. SPONSOR/MONITOR'S ACRONYM(S)**
U.S. Army Research Laboratory 2800 Powder Mill Road Adelphi, MD 20783-1197	**11. SPONSOR/MONITOR'S REPORT NUMBER(S)**

12. DISTRIBUTION/AVAILABILITY STATEMENT

Approved for public release; distribution unlimited.

13. SUPPLEMENTARY NOTES

14. ABSTRACT

A piezoelectric vibrational energy reclamation device using sol-gel PZT/surface micromachining technology is described for the low power supply of microsystems; converting environmental vibration into useful electrical energy for powering microsystems. The design is appropriate for the power generation of low power remote MEMS sensor network nodes. Electro-mechanical modeling, fabrication, and testing of PZT MEMS are presented. Power generation of 1.54 mW/cm^2 at 700 Hz/50 µm amplitude is predicted.

15. SUBJECT TERMS

Micro power; energy reclamation; piezoelectric

16. SECURITY CLASSIFICATION OF:			**17. LIMITATION OF ABSTRACT**	**18. NUMBER OF PAGES**	**19a. NAME OF RESPONSIBLE PERSON**
a. REPORT	**b. ABSTRACT**	**c. THIS PAGE**			Jeffrey S. Pulskamp
Unclassified	Unclassified	Unclassified	UL	21	**19b. TELEPHONE NUMBER** (*Include area code*) 301-394-0016

Standard Form 298 (Rev. 8/98)
Prescribed by ANSI Std. Z39.18

Contents

List of Figures

List of Tables

Acknowledgments

The author would like to thank Dr. Balakumar Balachandran**,** of the University of Maryland at College Park, and his graduate student Moustafa Al-Bassyiouni, for their help with and the use of his vibration table; Rich Piekarz and John Conrad for their work in device fabrication.

INTENTIONALLY LEFT BLANK

1. Introduction

Micro-power generation technologies have recently received a great deal of attention from both government laboratories and academia. The majority of the work under investigation today has focused on the miniaturization of macro-scale, fuel dependant power technologies such as micro-turbines (*1*) and micro-generators, (*2*). Micro-power technologies that use their environment for their sources of input energy (*3-6*), as opposed to requiring on board fuel, should provide the benefits of longer operational lifetimes and significantly lower system weight and volume. One detriment to these other approaches is the energy conversion loss associated with transformations from multiple energy domains. Microsystems that combust fuels (*7*), for example, transform energy from chemical to thermal to mechanical to electrical domains; the second law of thermodynamics dictates significant energy transformation losses that necessitate greater quantities of fuel, thus increasing the system size and volume and negatively impacting operational lifetimes. Piezoelectric vibrational energy reclamation requires only one energy transformation.

This work demonstrates the feasibility of vibrational energy harvesting via thin film PZT MEMS. Using the direct piezoelectric effect, periodic deflection of a piezoelectric thin film produces a generated charge that can be, for each deflection cycle, stored for later external system power requirements. The input energy is reclaimed from the waste vibrational energy of another mechanical system vibrating at a given frequency and amplitude. PZT is the piezoelectric thin film of choice for this application, given its superior electro-mechanical coupling coefficient (*8*).

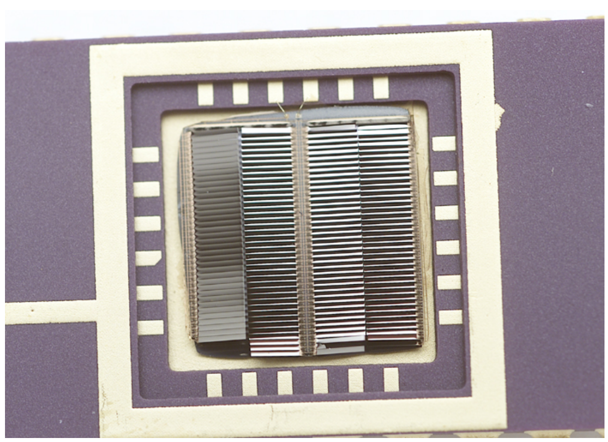

Figure 1. Prototype piezoelectric vibrational energy reclamation device.

We present analytical device modeling, MEMS fabrication, and the results from laser Doppler vibrometry and vibration testing. Piezoelectric charge generation derived from piezoelectric constitutive equations (*9*), a discretized Bernoulli-Euler mechanical deformation model, and simple power density derivation provide the basis for the modeling effort. Laser Doppler vibrometry (*10*) allows for the characterization of the device frequency response and resonant mode shape investigation, while the use of an electro-mechanical vibration table enables direct measurement of the piezoelectrically generated current. The basic geometry, coordinate system, and composition of the cantilever device are shown in figure 2.

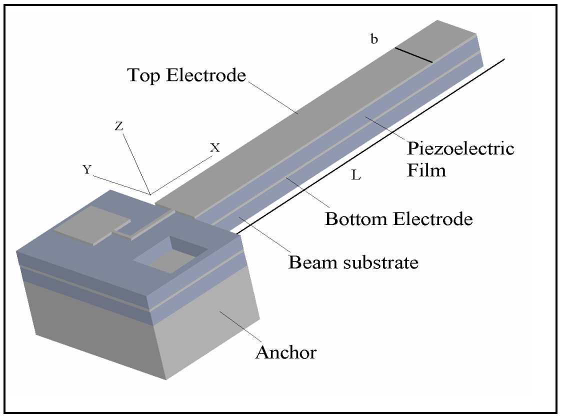

Figure 2. Conceptual cross-section of cantilever vibrational energy harvester, displaying coordinate system employed.

2. Vibrational Energy Reclamation Design

2.1 Piezoelectric Charge Generation

The charge generated by a piezoelectric cantilever beam is obtained by integrating the electric displacement perpendicular to the electrodes D_3 over the area of the beam. The following is an approximation of D_3:

$$D_3 \cong e_{31} h \mathrm{w}_{xx} \tag{1}$$

$$q_{\mathrm{piezo}} \cong \int D_3 b(\mathrm{x})\mathrm{dx} \tag{2}$$

$$q_{\mathrm{piezo}} \cong e_{31} h \int \mathrm{w}_{xx} b(\mathrm{x})\mathrm{dx} \tag{3}$$

The approximation arises from the presence of the h term, the distance from the neutral axis (N.A.) to the midplane of the piezoelectric layer. These expressions also assume uniform deformation across the width of the beam. By employing Bernoulli-Euler beam theory, the strain distribution is assumed linear with respect to the device thickness; implying the average strain is referenced by the h term. For a constant width electrode, equation 3 then becomes:

$$q_{\mathrm{piezo}}(\mathrm{t}) \cong e_{31} b h \Theta_{\mathrm{n}}(\mathrm{t}) \tag{4}$$

2.2 Bernoulli-Euler Mechanical Deformation Model

The devices are electrically coupled piezoelectric cantilever arrays. Modeling the basic cantilever structure as a Bernoulli-Euler beam permits the beam to be discretized into an arbitrary number of elements (FEM) with the deflections at each node described by, (*11*):

$$\begin{Bmatrix} v_i \\ \theta_i \end{Bmatrix} = \left[-[M]\omega^2 + [K]\right]^{-1} \begin{Bmatrix} F_i \\ M_i \end{Bmatrix} \tag{5}$$

where the vector on the left of equation 5 contains the vertical and angular displacements of each node (the last term is the angular deflection required to solve the charge equation 4). The vector on the right contains the amplitudes of the forces and moments at each node. Both vectors are (2n x 1) vectors where n is the number of nodes the beam has been discretized into. [M] and [K], the global mass and stiffness matrices, are assembled from their respective elemental matrices. For the one-dimensional case, the elemental matrices are assembled along the diagonal of an empty (2n x 2n) matrix, with adjoining nodal values summing. Equations 6 and 7 are the one-dimensional elemental mass and stiffness matrices; assuming a cubic shape function for the elements, (*11*).

$$[K_e] = \frac{EI_{comp}}{L^3} \begin{bmatrix} 12 & 6L & -12 & 6L \\ 6L & 4L^2 & -6L & 2L^2 \\ -12 & -6L & 12 & -6L \\ 6L & 2L^2 & -6L & 4L^2 \end{bmatrix} \tag{6}$$

$$[M_e] = \frac{mL}{420} \begin{bmatrix} 156 & 22L & 54 & -13L \\ 22L & 4L^2 & 13L & -3L^2 \\ 54 & 13L & 156 & -22L \\ -13L & -3L^2 & -22L & 4L^2 \end{bmatrix} \tag{7}$$

2.2.1 Conversion of Base Motion to Uniformly Distributed Inertial Harmonic Load

A cantilever beam subjected to harmonic motion of its base is acted upon by a uniform distributed inertial harmonic excitation force equal to equation 8, (*12*):

$$F = Y\omega^2 m_{\text{beam}} \sin(\omega t) \tag{8}$$

In order to represent this uniform distributed inertial load in the discretized Bernoulli-Euler equation of motion, the force must be adequately discretized along the length of the beam. In motion equation 5, the elemental force terms in the force and moment vector become the amplitude of F divided by the number of elements.

2.2.2 Determination of Composite Beam Modulus of Elasticity, Moment of Inertia, Unit Mass, Neutral Axis Location, and Resonance

The area moment of inertia of a cross-section of the beam with respect to the y-axis of the composite beam is the summation of the sums of the moments of inertia of each layer and the product of each layer's cross-sectional area and the square of the distance from the neutral axis to the centroidal axis of each layer, as given by the parallel axis theorem (*13*).

$$I_{\text{composite}} = \Sigma\,(I_{\text{i}} + A_{\text{i}}d_{\text{i}}^{2}) \tag{9}$$

The composite modulus of elasticity is the summation of the products of volume fractions of each layer and the modulus of the corresponding layer. For a constant width beam, this reduces to (*13*):

$$E_{\text{composite}} = \Sigma\,(t_{\text{layer}}E_{\text{layer}}/t_{\text{beam}}) \tag{10}$$

The location of the neutral axis is found by dividing the summation of the products of the layer cross sectional areas and the distances from the layer centroids to some arbitrary reference axis by the cross-sectional area of the entire beam, (*13*).

$$y_{\text{bar}} = (\Sigma\,(A_{\text{i}}y_{\text{i}}))/A_{\text{total}} \tag{11}$$

The mass per unit length is found by multiplying the beam width by the summation of the products of the layer densities and the layer thickness.

$$m_{\text{beam}} = b[\,\Sigma\,(\rho_{\text{layer}}t_{\text{layer}}\,)] \tag{12}$$

The natural frequencies of the beams are the eigenvalues of the following matrix expression:

$$[M]^{-1}\,[K]\{q_{\text{o}}\} = \omega_{\text{n}}^{2}\{q_{\text{o}}\} \tag{13}$$

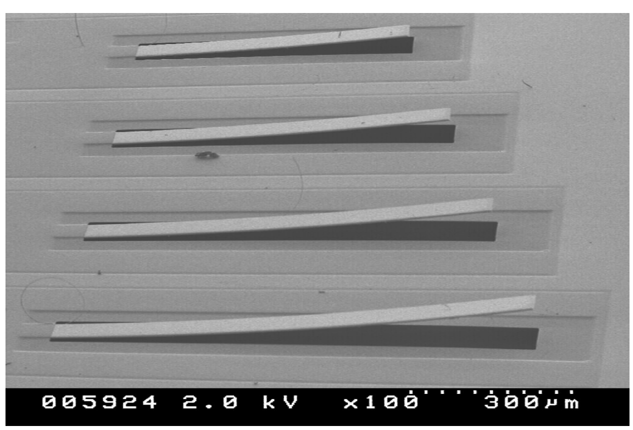

Figure 3. Micrograph of released cantilever test structures. Residual film stress deformation is apparent.

2.3 Power Density

The average power developed by a piezoelectric cantilever structure is equal to half of the maximum voltage across the PZT multiplied by the maximum current produced by the device. The voltage amplitude equation 16, across the PZT, is equal to the generated charge divided by the capacitance equation 14 of the PZT layer. Assuming that the charge is completely extracted once during the deflection cycle, the current amplitude equation 15 is the product of the operating frequency in hertz and the charge generated per deflection cycle.

$$C_p = (\varepsilon_{33}\, \varepsilon_o\, l\, b)/t_c \tag{14}$$

$$i_{piezo}(t) = q\, \omega\cos(\omega t) \tag{15}$$

$$V_{piezo}(t) = ((e_{31}\, h\, \Theta_n\, t_c)/(\varepsilon_{33}\, \varepsilon_o\, l))\sin(\omega t) \tag{16}$$

$$Power = (q\, i_{piezo})/2C_p \tag{17}$$

$$\mathrm{Power/Area} = (e_{31}\, h\, \Theta_n)^2\, \omega\, t_c / 2\varepsilon_{33}\, \varepsilon_o\, l^2 \tag{18}$$

2.4 Mitigation of Residual Stress Deformation

In order to investigate the behavior of the longer MEMS devices, on the order of a few millimeters, it was necessary to compensate for the residual thin film stress deformation of these highly compliant structures. If the mean force associated with the stress gradient, whose location can be determined from the mean value theorem of integrals, acts at a distance displaced from the structure's N.A., residual stress deformation will occur. This stress gradient, through the thickness of the device, leads to the distributed moment that serves to deform the structure out of plane. This deformation can be so extreme as to prevent either measurement of a device or even device operation. By designing the structure's film thicknesses and engineering the stress gradients, a near planar structure can be achieved.

3. Fabrication

We fabricated PZT-based cantilevers and cantilever arrays using a simple, four mask fabrication process. A schematic cross-section of a completed device is illustrated in figure 2. Starting with a bare Si wafer, a micron and a half of PECVD SiO_2 was deposited at 250 °C. The film was then annealed at 700 °C in a nitrogen atmosphere. An adhesion/diffusion barrier layer of titanium was sputtered on the PECVD oxide, followed by a sputtered platinum bottom electrode layer. Sol-gel $PZ_{0.52}T_{0.48}$ (PZT) was then repeatedly spun, pyrolized, and crystallized until the appropriate PZT thickness was achieved. A liftoff of sputtered platinum defined the top electrodes and bond pads.

Table 1. Thin film thickness for the devices tested; measured via Variable Angle Ellipsometry.

Material	Thickness (nm)
Silicon Dioxide	1688
Titanium	20
Bottom Platinum	120
PZT	2048
Top Platinum	100

After photo patterning, we defined the release trench and bottom electrode region by ion milling of the PZT. The remaining photoresist was ashed in an oxygen plasma. The now exposed platinum in the release trench and an electrical isolation trench were ion milled through the platinum and underlying SiO_2, exposing the underlying silicon substrate. After ashing, a fourth photolithography step defining the XeF_2 release windows was performed. Given the 1:1 etch aspect ratio of the XeF_2, the release windows were positioned a distance ½ the beam width from the anchors. This insured that the actual beam lengths corresponded to the designed lengths when the beams released. Device die were cleaved and released individually, undercutting the beams. After releasing in XeF_2, the photoresist was again ashed.

4. Experimental Results

Multiple devices and cantilever test structures with resonant frequencies from 570 Hz to 240 kHz were fabricated using the process flow described in section 3. The fabricated devices and test structures were packaged in forty pin dual inline package (DIPs), compatible with both testing apparatuses employed in device characterization, laser Doppler vibrometry and electro-mechanical vibration excitation. Figures 4(a) and 4(b) display the experimental setups used for this work.

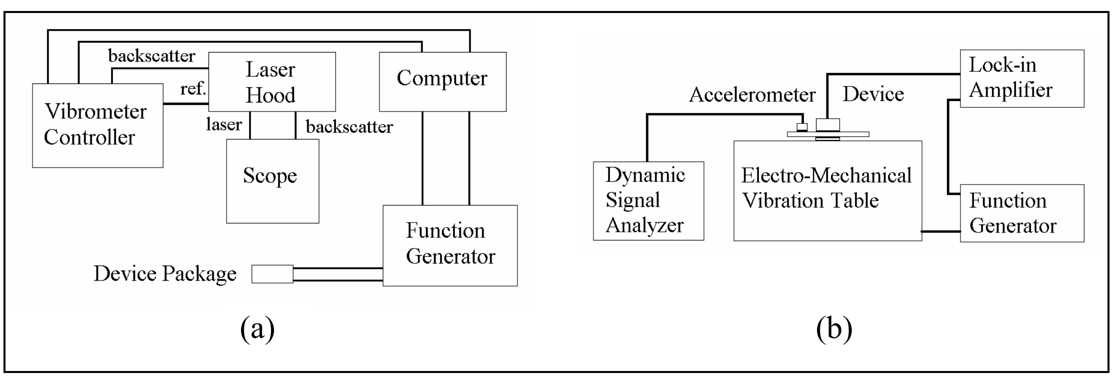

Figure 4. Block diagrams of the experimental setups used in characterizing piezoelectric vibrational energy reclamation devices; (a) laser Doppler vibrometer and (b) the vibration table.

4.1 LDV Frequency Response/Mode Shape Evaluation

The packaged devices were first characterized in terms of their frequency response. The devices were poled at their coercive field for approximately one hour. They were excited piezoelectrically at $1V_{p\text{-}p}$ and measured with a Polytec™ laser Doppler vibrometer at atmospheric pressure. A detailed discussion of this measurement technique can be found in other references (*10*).

Figure 5 and table 2 demonstrate good agreement between the eigen solutions of equation 13 and the LDV experimentally verified fundamental resonant frequencies. The underestimating of the natural frequencies may be due to a number of issues, including errors in the Young's modulus terms used in equation 13, the presence of residual film stresses (*14*), air damping, and deviation of actual beam length from designed/assumed lengths associated with the release process. Even with these uncertainties, the values are still within a few percent of experimental values.

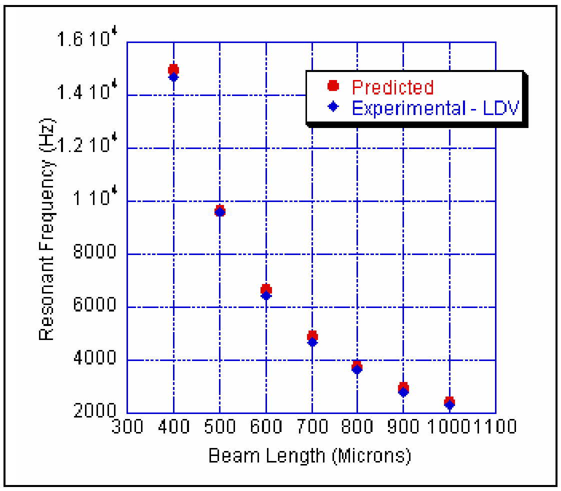

Figure 5. Experimental and predicted fundamental resonant frequency for varied cantilever beam lengths.

Table 2. Error between predicted and experimental fundamental natural frequencies.

Beam Length (Microns)	**% Error in Natural Freq.**
400	0.7
500	1.2
600	3.6
700	1.6
800	1.2
900	2.4
1000	1.25

The frequency response, up to 100 kHz, of a 2 mm long cantilever and an 1100 µm long cantilever are shown in figures 6a and 6b. The shift in predicted response is more apparent at higher frequencies, as the error (table 2) through higher order modes remains roughly constant.

In addition to frequency response behavior, laser Doppler vibrometry allows measurement of the resonant mode shapes. Figure 7 displays the fundamental harmonic, 7^{th} order mode shapes (region near the anchor only displayed due to scan area limitations) of a 2 mm long device, respectively. The observed mode shapes agree well with expectations. However, torsional modes of resonance (figure 7) were also observed. Their occurrence does appear to alter the measured frequency response, as the current model does not account for torsional modes. For the devices tested, torsional resonant modes are present in the range tested with the vibration table, as they were identified with the Laser Doppler Vibrometer. A more detailed investigation of these modes and their impact on the frequency response shall be pursued in future work.

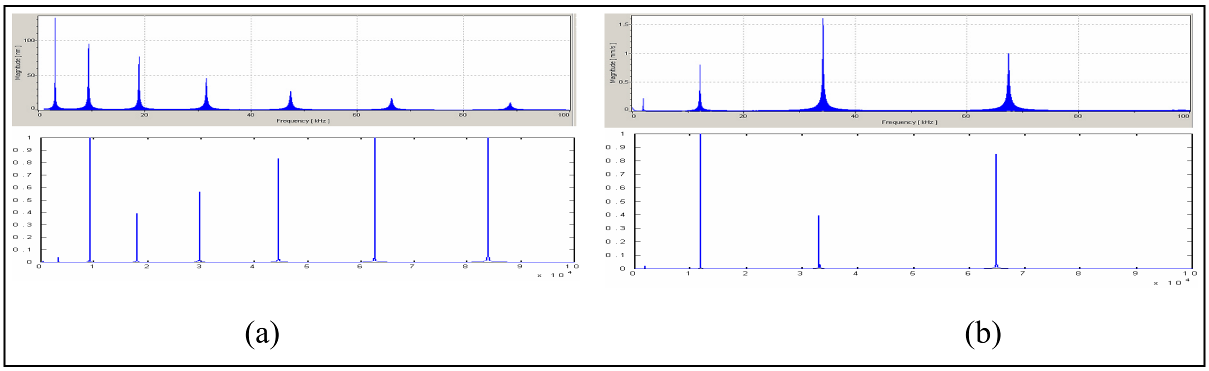

Figure 6. Experimental and predicted frequency responses of a 2 mm long (a) and an 1100 μm long device (b); the top plot in each is experimental data obtained from LDV while the lower plot is the predicted response w/arbitrary magnitudes.

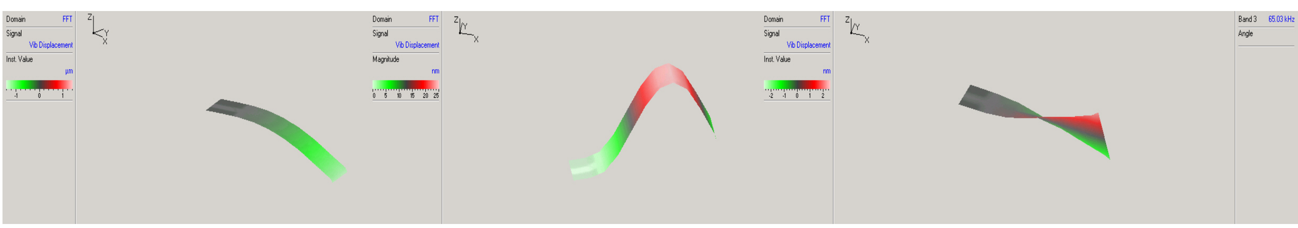

Figure 7. Fundamental, 7^{th} order, and torsional resonant mode shapes of a 2 mm long cantilever (only a portion near the anchor is actually visible).

4.2 Vibration Table Analysis

A B&K type 4808 vibration table, driven by a type 2712 power amplifier, was used to mechanically excite the piezoelectric cantilever test structure packages. The package was mounted in a specially designed fixture, containing a forty-pin zero insertion force (ZIF) socket, which allowed multiple packages to be tested with minimal work. An accelerometer was mounted to the fixture to measure the vibrational amplitudes. The table's fundamental resonance was 10.1 kHz, well above the range investigated. Data was taken between 100 Hz and 1 kHz, and at any resonance peaks present in the range. A lock-in amplifier was used to drive the table and to measure the generated piezoelectric current and voltage from the devices. As the amplitude of vibration was not easily decoupled from the frequency, the data displayed in figure 8, represents variable amplitudes of vibration. Figures 8a, 8b, and 8c display piezoelectrically generated current from vibration table testing for an 1100 µm long, 1500 µm long, and 2 mm cantilevers, respectively. There is reasonable agreement between the predicted and experimental currents. The deviation is thought to be due in part to the slight errors in resonant frequencies and the presence of torsional modes contributing to the frequency response.

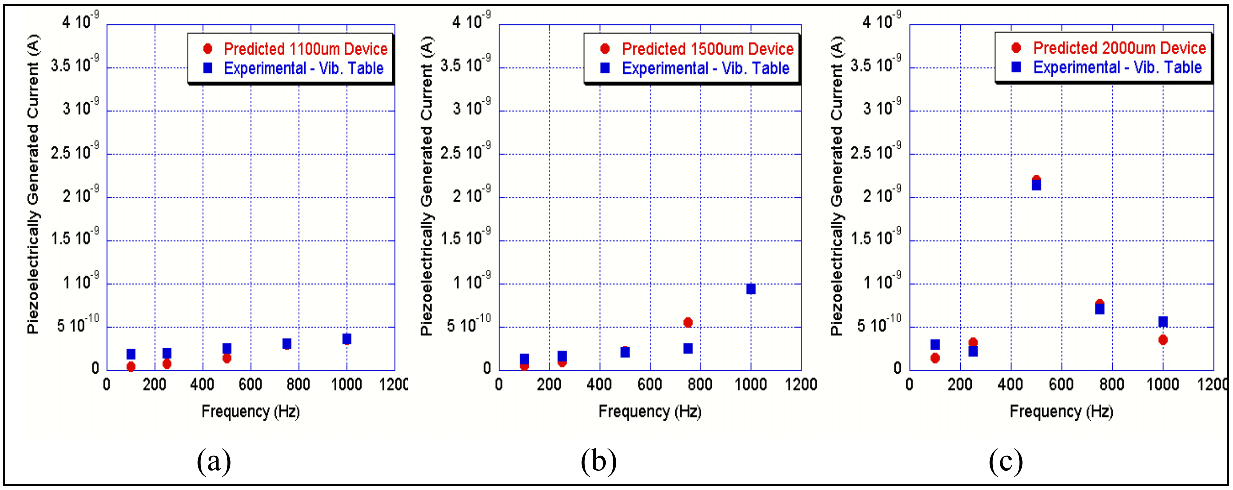

Figure 8. Piezoelectrically generated current for an 1100 µm long device (a), a 1500 µm long device (b), and a 2 mm long device (c) from vibrational excitation; model vs. experimental. Note: Displacement is coupled to frequency in the data.

The power generated at 570 Hz at a peak-to-peak displacement of 3.4 µm by the 2 mm long device was 0.16 nW. This translates into 0.08 $\mu W/cm^2$. The Laser Doppler Vibrometer and mechanical excitation testing of the prototype devices have demonstrated the validity of the current model. The model predicts power generation of 1.54 mW/cm^2 at 700 Hz/50 µm amplitude of vibration for an optimized device.

5. Conclusions

Surface micromachined piezoelectric PZT vibrational energy reclamation devices have been designed, fabricated, and tested to demonstrate the feasibility of vibrational energy reclamation via thin film PZT MEMS. Experimental data has validated the developed electro-mechanical model. Predictions of this model imply a power density of 1.54 mW/cm^2 at a 700 Hz, 50 µm amplitude vibration. Future work will focus on model optimization, development of an appropriate charge extraction circuit, and system demonstration.

6. References

1. Mehra, A.; et al. A six-wafer combustion system for a silicon micro gas turbine engine. *J. Microelectromechancial Systems* **2000**, *9*, 517.
2. Epstein, A. H.; Senturia, S. D.; .Al-Midani, O.; et. al. Micro-heat engines, gas turbines and rocket engines – the MIT Microengine Project. *AIAA* Paper 97-1773. Snowmass, CO. June 1997.
3. El-hami, M.; et al. Design and fabrication of a new vibration-based electromechanical power generator, *Sensors and Actuators A* **2001**, *A 92*, 335.
4. Amirtharajah, R.; Chandrakasam, A. P. Self-powered signal processing using vibration-based power generation, *IEEE J. Solid-State Circuits* **1998**, *33* (5), 687–695.
5. Williams, C. B.; Yates, R. B. Analysis of a micro-electric generator for microsystems, *Sensors and Actuators A* **1996**, *52*, 8–11.
6. Glosch, H.; et al. A thermoelectric converter for energy supply, *Sensors and Actuators A* **1999**, *74*, 246–250.
7. Mehra, A.; Waitz, I. A. Development of a hydrogen combustor for a microfabricated gas turbine engine, *J. MEMS* **2000**, *9*, 517–527.
8. Trolier-McKinstry, S. Manufacturable sol-gel PZT films for Microsensors and Microactuators; Final Technical Report, U.S. Army Contract DABT63-95-C-0053, 1998.
9. Ikeda, T. *Fundamentals of Piezoelectricity*, Oxford Science Publications: New York NY, 1996.
10. Sriram, P.; Hanagud, S.; Craig, J. I. Mode shape measurements using scanner laser Doppler vibrometer, *International Journal of Analytical and Experimental Modal Analysis* **1992**, *7*, 169–178.
11. Meirovitch, L. *Fundamentals of Vibrations*, McGraw-Hill: New York N.Y., 2001.
12. Den Hartog, J. P. *Mechanical Vibrations*, General Publishing Co.: Toronto Ontario, 1985.
13. Gere, J.; Timoshenko, S. P. *Mechanics of Materials*, PWS Publishing Co.: Boston MA, 1997.
14. Piekarski, B.; et al. Surface micromachined piezoelectric resonant beam filters, *Proc. Solid State Sensor and Actuator Workshop*, Hilton Head SC, June 2000.
15. He, J.; Fu, Z. *Modal Analysis*, Butterworth-Heinemann: Oxford MA, 2001.

INTENTIONALLY LEFT BLANK

Nomenclature

D_3	Electric displacement perpendicular to the electrodes
q_{piezo}	Piezoelectrically generated charge
N.A.	Neutral Axis
e_{31}	Piezoelectric stress constant
h	Distance from the N.A. to the PZT midplane
b	Beam width
w_{xx}	Beam curvature, 2nd derivative of deflection
x	Beam Axis dimension
Θ_{n}	Angular deflection at the free end of the cantilever beam
$[M]$	Global mass matrix
$[K]$	Global stiffness matrix
ω	Operating frequency in hertz
Y	Amplitude of vibration
q_o	Displacement Vector
m_{beam}	Mass of composite beam
F	Total inertial force
y_{bar}	Location of N.A. relative to arbitrary reference axis
E	Young's Modulus
I	Moment of Inertia
ρ	Mass density
t_{c}	Thickness of piezoelectric layer
ε_{33}	Piezoelectric layer dielectric constant
ε_{o}	Permittivity of free space (8.854×10^{-12} F/m)
i_{piezo}	Piezoelectrically generated current
l	Length of cantilever
C_{piezo}	Piezoelectric layer capacitance

Distribution List

ADMNSTR
DEFNS TECHL INFO CTR
ATTN DTIC-OCP (ELECTRONIC COPY)
8725 JOHN J KINGMAN RD STE 0944
FT BELVOIR VA 22060-6218

DARPA
ATTN IXO S WELBY
3701 N FAIRFAX DR
ARLINGTON VA 22203-1714

OFC OF THE SECY OF DEFNS
ATTN ODDRE (R&AT)
THE PENTAGON
WASHINGTON DC 20301-3080

US ARMY TRADOC
BATTLE LAB INTEGRATION & TECHL DIRCTRT
ATTN ATCD-B
10 WHISTLER LANE
FT MONROE VA 23651-5850

US MILITARY ACDMY
MATHEMATICAL SCI CTR OF EXCELLENCE
ATTN LTC T RUGENSTEIN
THAYER HALL RM 226C
WEST POINT NY 10996-1786

SMC/GPA
2420 VELA WAY STE 1866
EL SEGUNDO CA 90245-4659

US ARMY ARDEC
ATTN AMSTA-AR-TD
BLDG 1
PICATINNY ARSENAL NJ 07806-5000

COMMANDING GENERAL
US ARMY AVN & MIS CMND
ATTN AMSAM-RD W C MCCORKLE
REDSTONE ARSENAL AL 35898-5000

US ARMY INFO SYS ENGRG CMND
ATTN AMSEL-IE-TD F JENIA
FT HUACHUCA AZ 85613-5300

US ARMY NATICK RDEC
ACTING TECHL DIR
ATTN SBCN-TP P BRANDLER
KANSAS STREET BLDG78
NATICK MA 01760-5056

US ARMY SIMULATION TRAIN & INSTRMNTN CMND
ATTN AMSTI-CG M MACEDONIA
12350 RESEARCH PARKWAY
ORLANDO FL 32826-3726

HICKS & ASSOC INC
ATTN G SINGLEY III
1710 GOODRICH DR STE 1300
MCLEAN VA 22102

PALISADES INST FOR RSRCH SVC INC
ATTN E CARR
1745 JEFFERSON DAVIS HWY STE 500
ARLINGTON VA 22202-3402

DIRECTOR
US ARMY RSRCH LAB
ATTN AMSRD-ARL-RO-D JCI CHANG
ATTN AMSRD-ARL-RO-EN W D BACH
PO BOX 12211
RESEARCH TRIANGLE PARK NC 27709

US ARMY RSRCH LAB
ATTN AMSRD-ARL-CI-OK-T TECHL PUB (2 COPIES)
ATTN AMSRD-ARL-CI-OK-TL TECHL LIB (2 COPIES)
ATTN AMSRD-ARL-D J M MILLER
ATTN AMSRD-ARL-SE-RL J PULSKAMP (50 copies)
ATTN IMNE-ALC-IMS MAIL & RECORDS MGMT
ADELPHI MD 20783-1197